European Journal of Mechanics B/Fluids 29 (2010) 9–17

Contents lists available at ScienceDirect

European Journal of Mechanics B/Fluids

journal homepage: www.elsevier.com/locate/ejmflu

On the robustness of separation control by streamwise vortices

Ola Lögdberg [a,b,*], Kristian Angele [c], P. Henrik Alfredsson [a]

[a] Linné Flow Centre, KTH Mechanics, Royal Institute of Technology, S-100 44 Stockholm, Sweden
[b] Scania CV AB, S-151 87 Södertalje, Sweden
[c] Vattenfall Research and Development AB, S-162 87 Stockholm, Sweden

ARTICLE INFO

Article history:
Received 11 December 2008
Received in revised form
16 June 2009
Accepted 10 September 2009
Available online 18 September 2009

Keywords:
Adverse pressure gradient
Turbulent boundary layer
Flow separation
Flow control
Vortex generators

ABSTRACT

The robustness of vane-type vortex generators (VGs) for separation flow control was studied in a separating turbulent boundary layer on a flat plate. VG arrays of different sizes and streamwise positions were positioned upstream of the separation bubble and their effect on the flow field was studied with the help of particle image velocimetry (PIV). The extent of the separated region was varied by changing the pressure gradient. Three different separation bubbles were produced and their extent was approximately doubled for each increase in pressure gradient. It was found that the sensitivity of the control effect to changes in the size of the separation bubble is small within the applied range of pressure gradients. Furthermore, the importance of the relative position of the VGs with respect to the separated region is small.

1. Introduction

Turbulent boundary layer separation is a flow phenomenon which often has a great negative effect on the performance in many technical applications. Therefore, it is of great practical importance and there is much to be gained if separation can be controlled.

Schubauer & Spangenberg [16] investigated the relative performance of different mixing devices for separation control in a flat plate turbulent boundary layer subjected to a strong adverse pressure gradient (APG). Spanwise averaged mean velocity profiles were compared for different mixing devices and pressure gradients, and it was concluded that forced mixing has a similar effect as a reduction of the pressure gradient. Hence, forced mixing makes it possible to withstand a stronger pressure gradient, thereby delaying or even avoiding separation.

The most common technique to control separation in practice, on *e.g.* wings of commercial aircrafts, are vane-type VGs. Many different VG configurations were investigated by Pearcy [14] and design criteria were given for both cases with co-rotating and counter-rotating vortices. The latter configuration is used in the present investigation. In Fig. 1 the main VG parameters are defined.

Pearcy [14] predicted the vortex paths, based on inviscid theory for the interaction between different vortices and the surface (the image vortices). With a counter-rotating set-up, there is a transport of high momentum fluid from the free-stream towards the wall between two vortices from one VG pair, and there is a transport of low momentum fluid from the wall region up towards the free-stream between the two vortices from two different VG pairs. For this case the following was found: initially equidistant vortices approach each other in pairs with common outflow, which results in a movement away from the surface. If the vortices are arranged to be initially non-equidistant the two vortices from one VG pair move away from each other and towards the wall. The movement towards the wall was found to give a high maximum efficiency for separation control. However, eventually the vortices will reach an equidistant state, which will lead to a movement away from the wall. This scenario can be delayed by increasing the relative spanwise spacing (D/h) of the VG pairs, thus increasing the length over which the vortices are effective, at the expense of a slightly decreased maximum efficiency.

Pauley & Eaton [13] carried out measurements in a zero pressure gradient (ZPG) turbulent boundary layer using a VG height h of approximately 1.5 times the local boundary layer thickness δ. Focus was on the downstream development of the vortices in terms of streamwise vorticity ω_x and circulation Γ. For a vortex pair with common outflow it was found that at the streamwise position where the decay in Γ was approximately 50%, the maximum ω_x was reduced to 15–20% of its initial value. The

* Corresponding author.
E-mail address: ola@mech.kth.se (O. Lögdberg).

0997-7546/$ – see front matter © 2009 Elsevier Masson SAS. All rights reserved.
doi:10.1016/j.euromechflu.2009.09.001

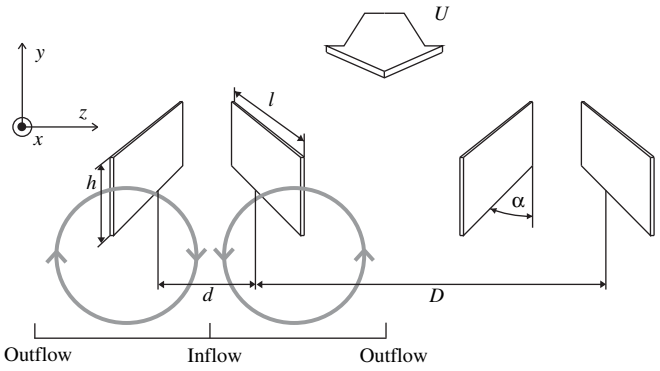

Fig. 1. VG geometry. All of the VG configurations used in this study produce counter-rotating vortices with a common inflow.

strength of the vortices increased linearly up to a VG vane angle of attack α of 18°.

Model predictions for the flow field induced by triangular wedge shaped VGs were made by Smith [17] to be used as a tool for VG design. The model predicted experimental data well and it was concluded that an increased efficiency could be realized by more dense VG arrays and by longer VGs. The most beneficial spanwise spacing was found to be $D/d = 2.4$, which is significantly lower than the $D/d = 4$, suggested by Pearcy [14].

More recent studies have focused on minimizing the drag induced by VGs, see e.g. the review by Lin [8]. A smaller VG results in lower form drag, making VGs with $h < \delta$ attractive, where δ is the boundary layer thickness. Lin, Howard & Selby [9] found that VGs with a relative height with respect to the boundary layer thickness $h/\delta = 0.1$ were effective but the circulation decayed rapidly.

Angele & Grewe [1] studied the behaviour of the streamwise vortices from a VG pair for the control of a separating APG boundary layer. It was found that the counter-rotating vortices from one VG pair moved away from each other in the spanwise direction and slightly outward in the wall-normal direction. The latter is contradictory to the conclusion by Pearcy [14], but is an effect of the viscous diffusion of the growing boundary layer and the growing vortices. The results from wall shear–stress measurements showed that an approximately two-dimensional state was reached at $(x–x_{VG})/h = 30$.

It was concluded by Angele & Muhammad-Klingmann [2] that the counter-rotating and initially non-equidistant streamwise vortices become and remain equidistant and are confined within the boundary layer, contradictory to the prediction by inviscid theory. The boundary layer developed towards a two-dimensional state in the downstream direction. A critical value was found for the ability to eliminate the backflow, above which an increase in the circulation only had a minor effect.

Godard & Stanislas [6] recently published a comprehensive optimisation study on co- and counter-rotating VGs, with $h < \delta$, in an APG boundary layer. They conclude that triangular blades are better than rectangular blades, both in terms of increased vortex strength and in reduced drag. They also found that the counter-rotating set-up was twice as effective as the co-rotating one in increasing the wall shear stress and that the optimum blade angle was $\alpha = 18°$.

Lögdberg, Fransson & Alfredsson [12] studied VG pairs and VG arrays in a ZPG wind tunnel experiment, and showed that the vortex core paths scale with h in the streamwise direction and with D in the spanwise directions. Furthermore the experimental data indicates that the vortex paths asymptote to a prescribed location in the cross-plane. This observation contradicts previously reported numerical results based on inviscid theory. An account for the important viscous effects is taken in a pseudo-viscous vortex model which is able to capture the streamwise core evolution throughout the measurement region down to $(x–x_{VG})/h = 450$.

1.1. Summary and present work

The present study is a continuation of Angele & Muhammad-Klingmann [2] and Lögdberg et al. [12] and aims at investigating the robustness of VGs for separation control. The question is how sensitive the control effect is to changes in the size and the location of the separation bubble relative to the VGs, something which is motivated by the changing nature of flows in real applications. More specifically we are investigating three cases with different strengths of the pressure gradients, generating separated regions of different extent. We also investigate the importance of the relative position of the VGs with respect to the separated region.

2. Experimental set-up

2.1. Wind tunnel

The experiments were made in the BL[1] wind tunnel at KTH Mechanics. The test section is 4.0 m long and has a cross-sectional area of 0.75 m × 0.50 m (height × width). A temperature control system makes it possible to keep the temperature constant within ± 0.03 °C. For a detailed description of the wind tunnel the reader is referred to Lindgren & Johansson [10]. A schematic of the experimental set-up is shown in Fig. 2. A vertical flat test plate made of Plexiglas spans the whole height and length of the test section and is mounted with its surface 0.30 m from the back side wall of the test section. The coordinate system origin is located at the centreline at the plate leading edge, with x in the streamwise direction, y in the wall-normal direction and z in the spanwise direction. At the leading edge the boundary layer is tripped in order to ensure a spanwise homogenous transition to turbulence. At the inlet the test section width is 0.5 m, but at $x = 1.25$ m the test section is diverged, by the back side curved wall, in order to decelerate the flow and thus induce an APG. The boundary layer thickness is approximately 21–24 mm, depending on flow configuration, at the start of the divergent part of the test section. Suction is applied on the curved wall to prevent the boundary layer from separating there. Instead the separation bubble develops on the flat test plate. By changing the suction rate the strength of the APG can be varied. Three different suction rates were used to create APG cases I, II and III. For APG case I the suction rate was set to 6–7% of the flow over the flat plate at the inlet of the test section. In case II the suction rate was 12.5–13% and in case III it was approximately 17%. Case I was thoroughly investigated by Angele & Muhammad-Klingmann [2,4] and case II and III are experiments performed in the present study. For definitions of case I, II and III see Section 3.1.1.

2.2. Measurement technique

All flow field measurements were performed with PIV in either x-y planes or x-z planes. The PIV-system uses a 400 mJ double cavity Nd:Yag laser operating at 15 Hz and a 1018 × 1008 pixels CCD camera with 8 bit resolution. The air was seeded with smoke droplets generated by heating glycol injected in the pressure equalizer slit downstream of the test section. The droplets are large enough to render a particle image size larger than 2 pixels in all measurements. According to Raffel, Willert & Kompenhans [15] this

[1] For "Boundary Layer" or "Björn Lindgren", after the designer of the tunnel.

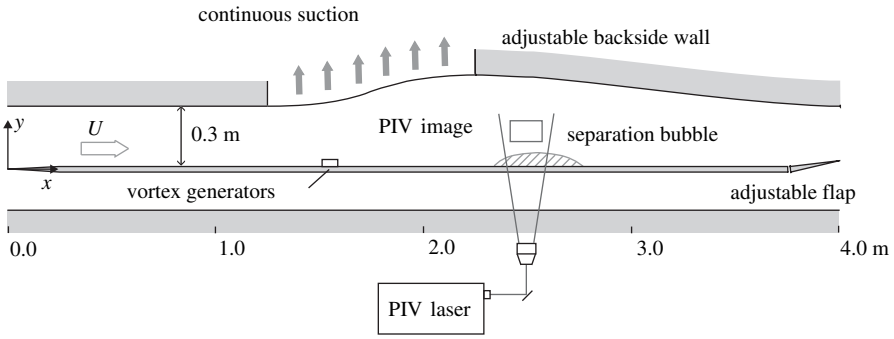

Fig. 2. Schematic of the test section seen from above. The x-direction is aligned with the test plate and the y-direction is perpendicular to it.

is enough to avoid peak-locking due to problems with the peak-fit algorithm. Furthermore, the ratio between the discretization velocity u_d and the u_{rms} is close to 2 in all measurements, which reduces errors due to peak-locking effects in mean- and rms-values to approximately 1% (Angele & Muhammad-Klingmann [3]). The number of particles inside the interrogation areas is higher than five, as recommended by Keane & Adrian [7], in all measured x-y planes. The maximum particle displacement corresponds to about 8 pixels.

The image size is approximately 150 mm and the error in the calibration of the image size is less than 0.5 mm, which gives an uncertainty of 0.3%. The statistical sampling error can be estimated by calculating the statistics based on n and $n-1$ samples. The convergence of the mean velocity in an arbitrarily chosen point in the flow is less than 0.5%, which indicates that the number of image pairs used here (1024) is sufficient in the present flow. The accuracy of the present PIV-data is estimated to be within 2% for the mean velocity and slightly worse for the higher statistics (not used for the analysis). Locally, close to the wall, the accuracy can be lower due to a large velocity gradient and reflections from the wall, however, the focus of the present paper is not on the near wall region, but on the large global changes in the flow with different VGs.

Conventional post-processing validation procedures were used. No particles moving more than 25% of the interrogation area length were allowed in order to reduce loss-of-pairs and the resulting low-velocity bias. The ratio between the highest and the second highest peak in the correlation plane must be more than 1.2 if the vector should be accepted. Often the light in the PIV images is streaky due to fittings and bubbles in the Plexiglas, but the streaks are always in the wall-normal direction at x-y plane measurements. Thus it was always possible to measure velocity profiles with validation ratios larger than 95%.

The wall static pressure P was measured on the test plate centreline in order to quantify the APG case. The Furness pressure transducer used, has an accuracy of 0.025% of full scale (2000 Pa), which in the present experiment gives a measurement accuracy of 1–3%. In Fig. 3 the pressure coefficient

$$C_p = \frac{P - P_{ref}}{P_0 - P_{ref}} \tag{1}$$

for the wall static pressure and its gradient in the flow direction are plotted against the distance from the leading edge of the test plate. P_{ref} is taken on the wall at $x = 0.45$ m and P_0 is the total pressure at the same x-position.

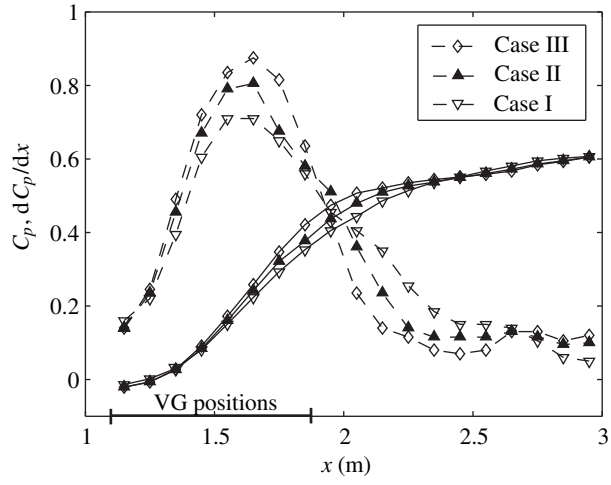

Fig. 3. Pressure distribution C_p and its gradient in the streamwise direction dC_p/dx. The region where the VGs are mounted is indicated on the x-axis.

2.3. The circulation generated by the VGs

In this experiment the separation control is performed by arrays of counter-rotating vortices, where each VG pair produces a vortex pair with common flow downwards (c.f. Fig. 1). All arrays span the whole width of the test section, like in Fig. 4. The VG arrays applied here have the same dimensions as the ones previously used by Angele & Muhammad-Klingmann [4], but are supplemented by one smaller set. Their geometries are described in Table 1. The blade angle α is 15° and the general design follows the criteria suggested by Pearcy [14]. There are four different sizes, that are geometrically self-similar, i.e. D/h, D/d and l/h are fixed (see Fig. 1).

For a VG pair, Angele & Muhammad-Klingmann [2] found that the total generated circulation can be estimated as

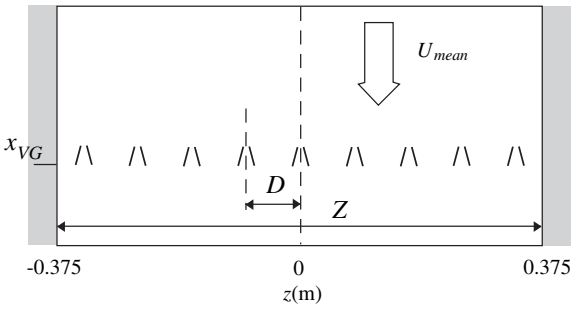

Fig. 4. A top-view of the 10 mm VG array in the BL wind tunnel. All tested arrays are set-up like this: the mid pair at $z = 0$ and the centreline of the outermost pair at a distance $D/2$ from the wall. The streamwise position of the array is defined as the position of the blade trailing edge.

Table 1
Physical dimensions of the VG sets. The first parameters are defined in Figs. 1 and 4, Z is the width of the test section and Z/D is the number of VG pairs in the array.

h (mm)	d (mm)	l (mm)	D (mm)	l/h	D/h	D/d	Z/D
6	12.5	18	50	3	8.33	4	15
10	21	30	83	3	8.33	4	9
18	37.5	54	150	3	8.33	4	5
30	62.5	90	250	3	8.33	4	3

$$\Gamma_e = 2khU_{VG}, \tag{2}$$

where U_{VG} is the mean velocity at the VG blade tip and k is a coefficient which is a function of the geometry of the VG. The estimation of Γ makes it possible to rank the circulation of different VG configurations without measuring the velocities in the y-z plane. For an array of VGs, it is better to estimate the circulation generated per unit width

$$\gamma_e = 2k\frac{hU_{VG}}{D}. \tag{3}$$

For the VG array the number of VGs increases with decreasing blade height, but h/D is constant. However, γ_e increases with h since the blade reaches higher up in the boundary layer, where the velocity is higher. For the VG geometry described in Table 1, Eq. (3) becomes $\gamma_e = 0.24kU_{VG}$.

In Lögdberg et al. [12] the cross-plane velocities produced by VG arrays, identical to the ones applied here, were measured in a plane $6h$ downstream of the array. The circulation was calculated by integrating the streamwise vorticity ω_x over an area. The total circulation Γ_{tot} is obtained by integrating ω_x over one half of a wavelength ($\Delta z = D/2$) in the spanwise direction. To obtain Γ_Q an integration of ω_x is made over the area inside a contour defined by a constant value of Q_x. Q is the second invariant of the velocity gradient tensor, and its streamwise component is calculated as

$$Q_x = -\frac{1}{2}\frac{\partial W}{\partial y}\frac{\partial V}{\partial z} \tag{4}$$

in the y-z plane. Q_x is useful since it is a measure of the local rotation, without contribution from pure shear. The contour of constant Q_x is chosen as $Q_x = 0.05 \cdot Q_{x,max}$. This level is somewhat arbitrary, but empirical tests have shown that this value produces stable and consistent levels of circulation for a wide range of data. In Fig. 5(a) the circulation measured for $h = 6$, 10 and 18 mm, in Lögdberg et al. [12], are compared to the corresponding circulation estimates from Eq. (2). The figure shows that $k = 0.6$ produces a good agreement between the measured Γ_Q and the circulation estimate. For the results presented here the value of k is less important and it is sufficient that the estimate works in a consistent way when comparing the relative strength of the vortices produced by different VG configurations. However, since Γ_Q is considered the best measure of the vortex circulation, $k = 0.6$ is used in the results presented hereafter, thus $\gamma_e = 0.144U_{VG}$.

In the present study, the circulation generated by the VG array is varied by varying h and x_{VG}. Changing h directly affects Eq. (3), but x_{VG} acts by changing U_{VG}. When the position of the VG array is moved downstream, the rapidly increasing boundary layer thickness δ causes h/δ to decrease and thereby reduces U_{VG}. In this region the decreasing U_e also causes U_{VG} to decrease downstream. The VG array was positioned at different locations in the region $1.10\text{ m} < x_{VG} < 1.95\text{ m}$ in order to generate different levels of circulation. To be able to estimate γ_e, 15 wall-normal velocity profiles were measured in this region. Then γ_e was calculated for four different values of h at each measurement position, using Eq. (3). The resulting values of γ_e for case III are shown in Fig. 5(b). The lines are least squares fits to the points.[2] Note that for the largest VGs, $h > \delta$ for $x < 1.5$ m and thus γ_e no longer increases as x_{VG} is moved upstream.

3. Results

In the following section the experimental results are presented. First the uncontrolled flow cases are characterized. Then the effects of different VG array configurations are reported. The shape factor $H_{12} = \delta_1/\delta_2$, where δ_1 is the displacement thickness and δ_2 is the momentum loss thickness, is consistently used to describe the boundary layer.

3.1. The uncontrolled case

The uncontrolled APG cases are also discussed in Lögdberg, Angele & Alfredsson [11]. The free stream velocity in the wind tunnel U_∞ is 26.5 ± 0.1 m/s at the inlet of the test section. The temperature was kept constant at 20 °C throughout all the measurements.

3.1.1. The pressure distribution and the shape factor

The pressure gradient was set through a contoured wall and by changing the suction rate as described in Section 2.1. Three pressure gradients are compared here. Data for case I are taken from Angele & Muhammad-Klingmann [2,4] and are reproduced here. Case II and III are new experiments. Case I is a weak separation bubble, case III is the largest possible separation bubble with the present suction fan and geometry and case II is in between the other two pressure gradients. Case II is the most thoroughly investigated configuration.

As shown in Fig. 3 the APG reaches its maximum between $x = 1.6$ and 1.7 m. In this area the maximum dC_p/dx for the three APG cases are 0.70, 0.78 and 0.87 m^{-1} respectively. The shape factor is approximately constant until $x = 1.7$ m for all three cases, as shown in Fig. 6. Then it increases rapidly and reaches a maximum at $x \approx 2.55$ m.

3.1.2. The backflow coefficient

Here the separation bubble is defined as the region where backflow occurs more than 50% of the time ($\chi > 0.5$). The point of separation is defined as the position where the backflow coefficient on the wall[3] (χ_w) reaches 0.5. This parameter is difficult to measure directly with PIV, since the interrogation areas must be large enough to contain approximately 5 particles. In this experiment the data points closest to the wall are located at $y = 1.5$–3 mm, and since χ is a strong function of y, the value of χ measured at the point closest to the wall under-predicts χ_w. Dengel & Fernholz [5] used wall pulsed wires with the sensor wires only 0.03 mm above the wall to obtain an accurate value of χ_w. According to their data, χ is almost a linear function of y when χ_w is larger than 0.4–0.5. Therefore, χ_w was estimated from a linear fit to the seven data points closest to the wall, as shown in Fig. 7(a). The described procedure will still under-predict χ_w for lower values of χ_w, but in the separation bubble χ_w is more accurate. In Fig. 7(b) the development of χ_w through the separated region is shown for APG case II.

3.1.3. Overview of the separated region

The set-up aims at a two-dimensional flow around the test section centreline ($z = 0$) and the spanwise velocity profiles in Fig. 8 show an acceptable two-dimensionality even for the worst case (III).

[2] By extrapolating the curves to $\gamma_e = 0$, it is possible to obtain a fairly accurate estimate of the separation point.

[3] On the wall it is the direction of τ_w that defines χ.

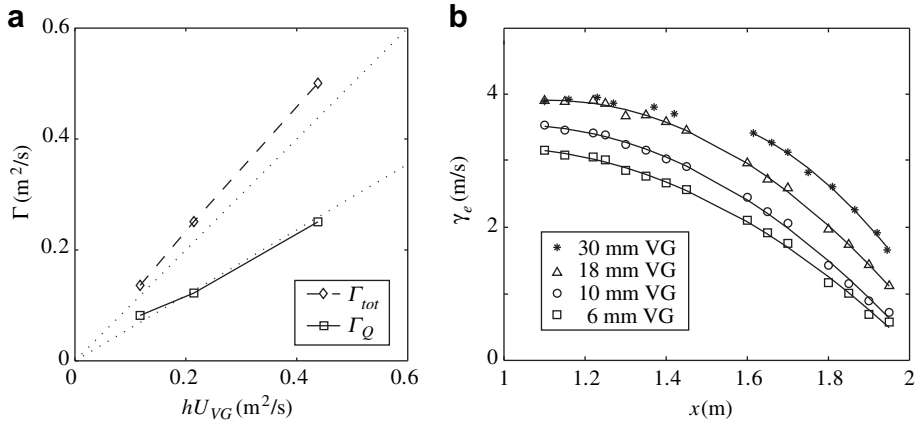

Fig. 5. (*a*) Circulation generated by 6, 10 and 18 mm VGs calculated in two different ways from the ZPG data of Lögdberg et al. [12]. The two dotted lines show $k = 0.6$ and $k = 1.0$ in Eq. (2). (*b*) Estimated generation of circulation per unit width depending on the position and size of the VG in APG case III for the arrays described in Table 1.

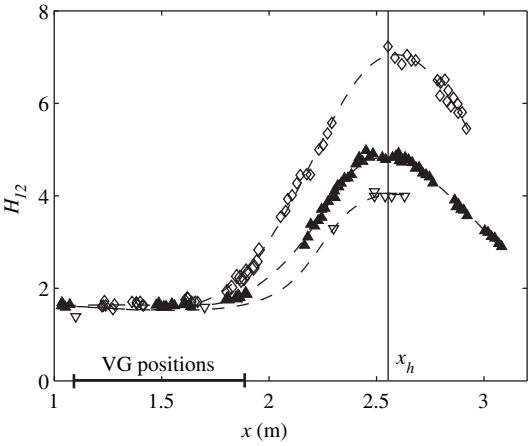

Fig. 6. Streamwise evolution of H_{12}. Note that the lines are for visual aid only.

An overview of the three investigated separation bubbles is given in Table 2, where x_s and x_r are the separation and reattachment points, respectively, l_s is the length of the separated region and h_s its maximum height. Here x_r is defined in the same way as x_s, *i.e.* $\chi_w = 0.5$. When the pressure gradient increases, x_r is moving downstream approximately the same distance as x_s is moving upstream and the position of the separation bubble centre is thus nearly constant for all cases. The bubble size (both l_s and h_s) is approximately doubled in between the APG cases. Furthermore, the bubble aspect ratio *AR*, *i.e.* ratio of height to length, increases with increasing pressure gradient. Thus the separation bubble thickness increases both in absolute and relative terms with increasing APG. Also $H_{12,sep}$, which is H_{12} at x_s, increases with increasing APG.

Case II is most thoroughly investigated and an overview of the flow around the separation bubble is shown in Fig. 9. In the figure the streamwise evolution of the mean velocity profile and the backflow coefficient are presented. A complete profile at each position was obtained from two measured *x*-*y* planes, which overlap slightly in the *y*-direction. As reported in Table 2, $x_s = 2.24$ m and $x_r = 2.85$ m. Note that, due to the growth of the boundary layer, the *y* position where $\chi > 0$ is moving further out from the wall even after the bubble has passed its maximum height. The first backflow events occur a short distance upstream of the separation point, and from Fig. 7(*b*) the position can be estimated to be at $x \approx 2.1$ m.

The mean velocity profiles for all three cases at $x = 2.55$ m are compared in Fig. 10. In Lögdberg et al. [11] it was shown that the mean velocity defect profiles of the three APG cases are self-similar in the region between x_s and the position of maximum backflow.

3.2. The controlled case

As shown in 5(*b*), the rapidly growing boundary layer makes it possible to produce vortex strengths up to $\gamma_e = 4.0$ m/s for 30 mm

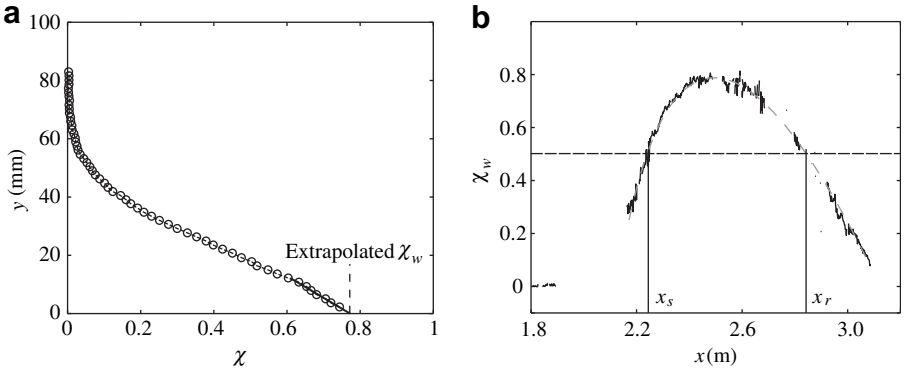

Fig. 7. (*a*) The backflow coefficient at the wall for case II. χ is extrapolated to the wall from the data points in the region $y \approx 1.5$–10 mm, to estimate χ_w. (*b*) The downstream development of χ_w for case II. The dashed line indicates $\chi_w = 0.5$.

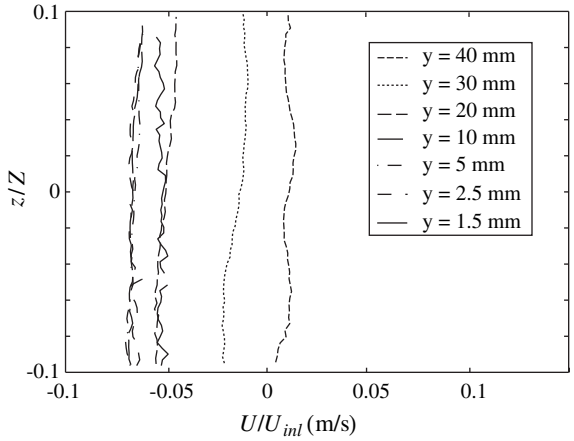

Fig. 8. Mean velocity profiles at $x = 2.55$ m for case III.

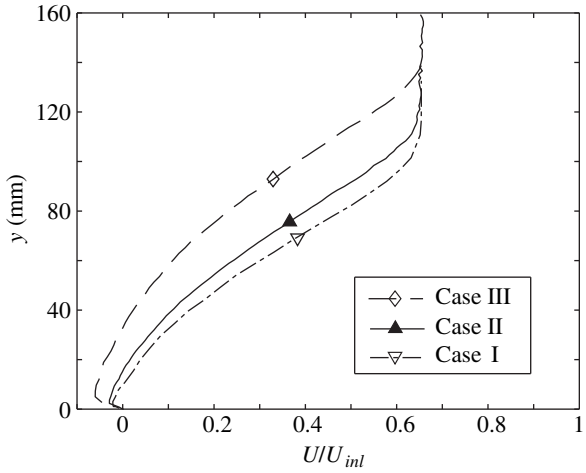

Fig. 10. The mean velocity profiles at $x = 2.55$ m in the uncontrolled APG cases.

Table 2
Separation bubble size. In case III the point of reattachment is approximated from visual inspection of tufts attached with tape on the test plate. Thus x_r and l_s are more uncertain for case III.

Case	dC_p/dx (m^{-1})	x_s (m)	x_r (m)	l_s (m)	h_s (mm)	$H_{12,sep}$	AR
I	0.70	2.4	2.7	0.3	7	3.45	0.23
II	0.78	2.24	2.85	0.6	17	3.50	0.28
III	0.87	2.09	3.1	1.0	35	3.75	0.35

and 18 mm VGs, $\gamma_e = 3.5$ m/s for 10 mm VGs and $\gamma_e = 3.1$ m/s for 6 mm VGs. However, in relation to the measurement position, the vortices produced further upstream will evolve and decay over a larger distance compared to vortices produced at a position further downstream. This is discussed in Section 3.2.3.

3.2.1. Measurement positions

In Fig. 6 it is shown that the maximum in H_{12} occurs at $x_h \approx 2.55$ m for all APG cases. Furthermore, in Lögdberg et al. [11] it was reported that H_{12} increases linearly with χ_w and that their maxima coincides. Thus x_h is suitable as reference position when the control effect of different VG sets is compared. The spanwise position where the vortices produce an inflow is always at $z/D = 0$ and the outflow position is at $z/D = 0.5$. Since these are the extreme positions, velocity profiles are always measured at both $z/D = 0$ and $z/D = 0.5$. Detailed results from APG case I are thoroughly presented in Angele & Muhammad-Klingmann [2] and the focus of the present paper is on case II and case III.

3.2.2. Circulation and reverse flow elimination

When evaluating the control effect of the vortices it is useful to define a simple measure of merit. The measure used in this article is H_{12}. In separated flows H_{12} is a good indicator of the backflow. It has been shown by Dengel & Fernholz [5] and Lögdberg et al. [11] that H_{12} is proportional to χ_w in the separated region. In this experiment H_{12} and χ_w are nearly proportional also in the flow cases with VGs. It could be argued that χ_w is more suitable for separation control purposes. The reason why H_{12} is preferred is that it is easier to calculate it accurately for $\chi_w < 0.4$–0.5.

The purpose of the VG arrays is to eliminate the mean reverse flow in the separated region. In Fig. 11 the streamwise mean velocity profiles $U(y)$ at the position of inflow ($z/D = 0$) and the position of outflow ($z/D = 0.5$) at x_h, are shown for different VG configurations in case II. The uncontrolled case, $\gamma_e = 0$, is shown for comparison. In Table 3 the results are listed. At the position of inflow, more streamwise momentum is transported down through the boundary layer, and a larger effect of the VGs can be seen compared to the position of outflow. However, due to the spanwise movement of the vortices and the viscous diffusion, the difference has become quite small. The two VGs which produces the least circulation, $\gamma_e = 0.8$ and $\gamma_e = 1.0$, have negligible influence on U, but when the circulation is increased to $\gamma_e = 1.4$ mean separation is prevented. The change in U is not large, but as shown in Fig. 12 the reverse flow is almost eliminated. At the positions of inflow and outflow χ_w is only about 0.08 and 0.15 respectively. Thus, the backflow coefficient is correlated to the circulation in a nonlinear way. Since the drag of the VG array is expected to increase with γ_e,

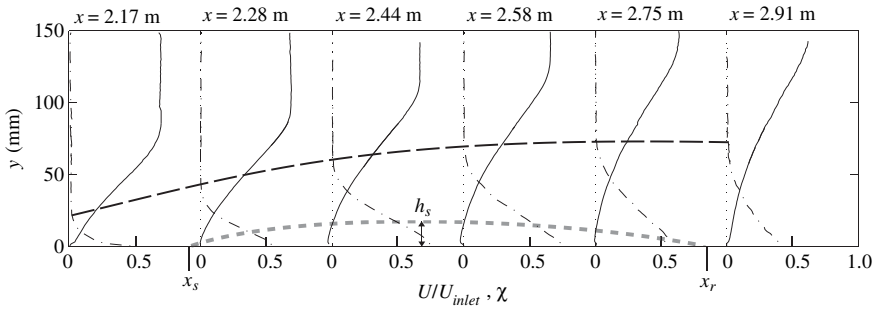

Fig. 9. The separation bubble for the APG case II. The figure is not to scale and therefore the bubble appears to be thicker. The full lines show U/U_{inlet}, the dash–dotted lines show the backflow coefficient χ. The extent of the separation bubble, defined as the region where $\chi > 0.5$, is shown by the lower dashed line. The higher dashed line shows the region of $\chi > 0$.

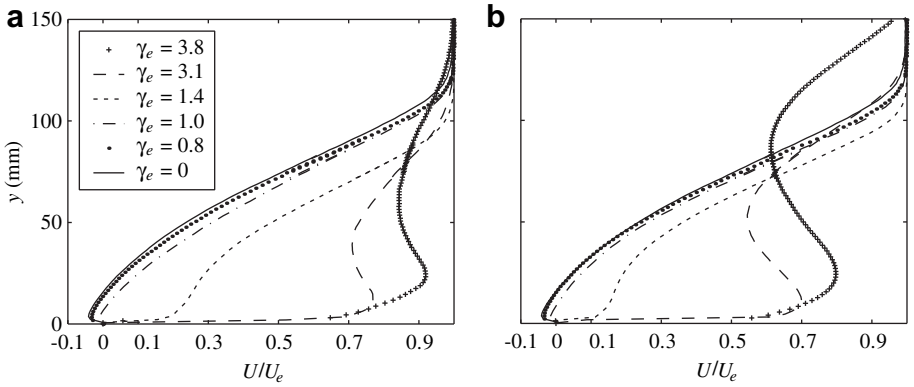

Fig. 11. Mean velocity profiles at (*a*) the spanwise position of inflow and (*b*) the position of outflow.

Table 3
H_{12} and χ_w of the profiles seen in Figs. 11 and 12.

γ_e (m/s)	x_{VG} (m)	h (mm)	$(x_h - x_{VG})/h$	H_{12}		χ_w	
				Inflow	Outflow	Inflow	Outflow
0	–	–	–	4.9	4.9	0.75	0.75
0.8	2.0	6	92	4.6	4.9	0.74	0.75
1.0	2.0	10	55	4.0	4.4	0.63	0.65
1.4	2.0	18	31	2.6	3.2	0.11	0.13
3.1	1.6	18	53	1.4	1.6	0.0	0.0
3.8	1.1	18	81	1.3	1.5	0.0	0.0

this is the most efficient VG configuration for preventing separation in this particular flow case.

Fig. 13 summarises the separation control effectiveness of all examined VG configurations. Here the H_{12} values at x_h for case I, II and III are compared for different γ_e. In the separation bubbles of the uncontrolled cases, H_{12} is approximately 4, 5 and 7 in the respective cases. This can also be seen in Fig. 6. The dashed lines display the results at the spanwise position of outflow and the dotted line refers to the position of inflow. A fuller profile and hence a lower H_{12} is expected at the position of inflow, as can be seen when comparing Fig. 11(*a*,*b*). This is shown in Fig. 13, where the two curves are separated by an average $\Delta H_{12} \approx 0.3$.

For the flow to stay attached ($\chi_w < 0.5$), H_{12} should be lower than $H_{12,sep}$ in Table 2, *i.e.* $H_{12} \approx 3.5$. The light grey area in Fig. 13 indicates the present range of $H_{12,sep}$. The value of γ_e at which the flow stays attached seems to be fairly insensitive to the pressure gradient, even though the difference in size of the separated region is quite large in the uncontrolled cases. The drop in H_{12} is sudden in both case II and III, and confirms the nonlinearity suggested above. When the circulation is further increased, the shape factor levels off to about $H_{12} = 1.3$ at the position of inflow and to $H_{12} = 1.5$ at the position of outflow. Thus the average H_{12} seems to asymptotically approach 1.4, similarly to a ZPG turbulent boundary layer, even though the shape of the velocity profile is different. At $\gamma_e > 1.5$ m/s the variation of H_{12} with γ_e is similar for all APG cases, and for $\gamma_e > 2.5$ m/s the pressure gradient has no effect on H_{12}. This suggests that there exists a γ_e, within the present APG range, above which the pressure gradient no longer affects the flow.

3.2.3. Streamwise position of the VGs

To design an efficient flow control system with VGs it is not only necessary to decide the circulation required to prevent separation, but also the position of the VGs with respect to the point of separation. So far, in the present study, it has not been taken into account at which position γ_e is generated. The position is important since the circulation decays in the downstream direction and also since the location of x_s might change.

In Lögdberg et al. [12] the decay of the streamwise circulation of vortices, produced by VG arrays identical to the present ones was measured in a ZPG turbulent boundary layer. As shown in Fig. 14(*a*) the circulation decay scales with h. Since the APG changes the boundary layer in which the vortices are embedded it is reasonable to assume that the rate of decay might change. However, Westphal et al. [18] reported that even though the vortex core grows quicker in an APG and the peak vorticity becomes lower, the decay of circulation from a vortex with the same initial circulation does not change when a pressure gradient is imposed.

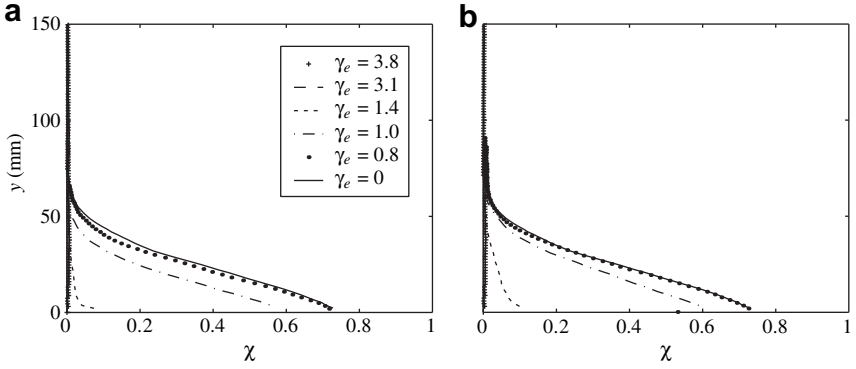

Fig. 12. Backflow coefficient profiles at (*a*) the spanwise position of inflow and (*b*) the position of outflow.

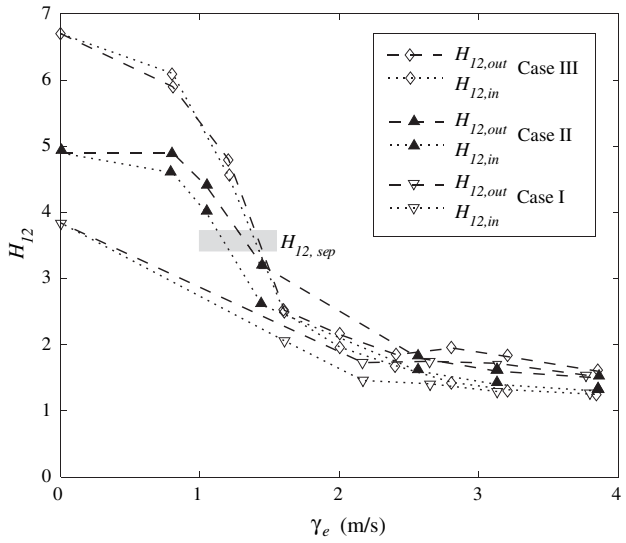

Fig. 13. The shape factor H_{12} at the position of inflow and the position of outflow plotted against γ_e in case I, II and III. The measurements were made at the respective separation bubble's streamwise position of maximum bubble height.

In Fig. 11 the vortices of $\gamma_e = 3.8$ are produced by a VG array at x_h–$x_{VG} = 81h$, whereas the vortices of $\gamma_e = 1.4$ are generated at x_h–$x_{VG} = 31h$. Assuming that the decay of circulation displayed in Fig. 14(a) is applicable, the stronger vortices would have lost 60% of their estimated circulation at x_h, while the weaker vortices would have lost only about 20% of their circulation. The question is if it is γ_e at x_h which is of importance for separation control purposes or if it is the initial γ_e. Primarily, the boundary layer's capacity to withstand an APG depends on the fullness of the velocity profile. Fig. 14(a) should not be interpreted as showing the decay of the control effect. High momentum fluid is transported towards the wall despite the fact that the circulation decays, when the vortices are convected downstream. Also the downward momentum transport thus takes place over a longer streamwise distance for VG configurations positioned further upstream. Therefore there are two seemingly opposing consequences when the streamwise position of the VG array is moved upstream: a decreased circulation at x_h and an increased total momentum transport towards the wall.

Table 4
Four VG configuration that produce $\gamma_e = 3.1$.

h (mm)	x_{VG} (m)	$(x_h$–$x_{VG})/h$	γ_e (m/s)
6	1.10	242	3.1
10	1.37	118	3.1
18	1.54	56	3.1
30	1.68	29	3.1

In order to investigate the influence of the streamwise position of the VG array on the control effect, the same magnitude of circulation was produced at four different x-positions. This was accomplished by applying the 6, 10, 18 and 30 mm VGs at different streamwise positions so that hU_{VG} is constant (see Table 4). The procedure is illustrated in Fig. 14(b), which is based on the data from Fig. 5. Two arrays are placed before the pressure gradient peak

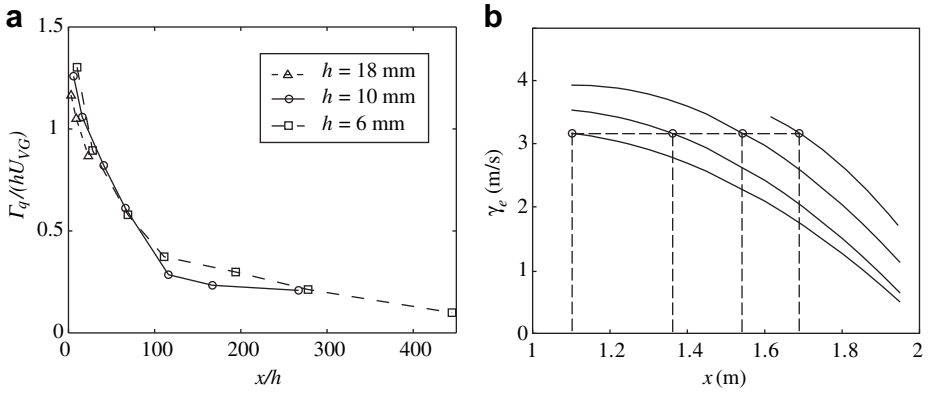

Fig. 14. (a) Circulation decay downstream of arrays of VGs in ZPG (b) γ_e generated by the four different VG sizes in case III. The horizontal line indicates $\gamma_e = 3.1$ and the x-positions where it intersects with the four lines of estimated circulation shows where the VGs should be placed to generate $\gamma_e = 3.1$.

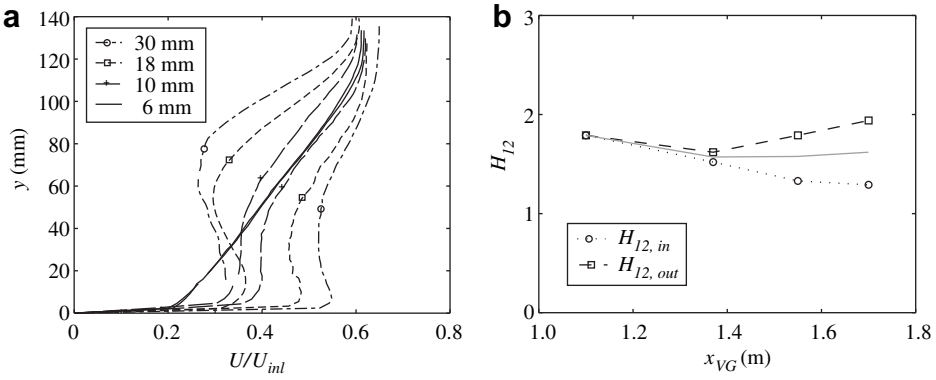

Fig. 15. (a) Mean velocity profiles at the spanwise positions of inflow and outflow for four different VG configurations described in Table 4. The four rightmost profiles are measured at the position of inflow and the others at the position of outflow. (b) H_{12} measured at x_h for an estimated generated γ_e of 3.1 m/s. The circulation is produced at four different x-positions. The upper curve is H_{12} at the position of outflow and the lower curve is H_{12} at the position of inflow. The grey line shows the mean H_{12}.

in Fig. 3, one is placed at the position of the peak and one is positioned right after the maximum in the pressure gradient. The normalised distance from x_{VG} to x_h span $x/h = 29$–242.

In Fig. 15(a) the resulting mean streamwise velocity profiles at the spanwise positions of inflow and outflow at x_h are presented. For the case with 6 mm VGs the boundary layer has become two-dimensional. With the 10 mm VG array, the velocity profiles at the positions of inflow and outflow are slightly shifted with respect to each other, with a fuller profile at the position of inflow. For the next two cases of larger VGs and decreasing x/h, the shift of the profiles at the inflow and outflow positions increases further, showing that they have not developed as far. However, if an average of the profiles at the inflow and outflow positions are taken for each VG size, the resulting velocity profiles of the three largest VGs become quite similar. Hence, H_{12} of the average mean velocity profiles are similar. This is shown in Fig. 15(b), where H_{12} at the inflow and outflow positions are plotted against x_{VG}. The grey line in the figure shows the average H_{12} of both spanwise positions and one can conclude that the control effect in terms of H_{12} at x_h, is insensitive to the streamwise position and dP/dx for x_h–$x_{VG} = 29h$–$118h$. For the most upstream VG array at x_h–$x_{VG} = 242h$ the control effect is reduced (see Table 4 for the conversion between x_{VG} and $(x_h$–$x_{VG})/h$). Note that the resulting data points in Fig. 13 are all within the x_{VG}-insensitive range.

4. Conclusions

In this study the control effectiveness of conventional vane-type VGs has been investigated, for different pressure gradients and different levels of generated circulation, using PIV.

As the circulation is increased the effect on the separated region is first small, but when a critical γ_e is reached the flow does not separate. Since the parasitic drag of the VGs increases with γ_e, the lowest possible γ_e that still keeps the boundary layer attached is the most efficient. This, together with the sudden change to attached flow produces a pronounced efficiency maximum. However, in an application where the flow conditions vary, a system designed for maximum efficiency might be sensitive to such variations and therefore not practical.

Fig. 13 illustrates the sensitivity of the VG system. For maximum efficiency a control system should be designed to produce the lowest possible γ_e that prevents separation. If a change of the flow at x_{VG} causes U_{VG} and γ_e to decrease, the flow at x_h can quickly become separated. Thus, an optimised system is sensitive to variations in γ_e. However, if instead the pressure gradient changes, Fig. 13 shows that the effect is small. Thus, the VG system is not sensitive to variations in the pressure gradient.

In Fig. 15(a,b) it is shown that, within a range of x_h–x_{VG}, the streamwise position of the VG array is of minor importance. Thus, the VG system is not sensitive to changes of the separation point. However, note that the more full velocity profiles produced by the VGs increases the wall friction. Since a more upstream position of the VGs increases the streamwise length of higher wall friction it also increases the drag.

To conclude, flow control by means of vane-type VG arrays is robust with respect to changes in the pressure gradient and changes of separation point. However, if the system is designed for optimum efficiency it could be sensitive to changes of the flow conditions at the position of the VG array.

Acknowledgements

Ola Lögdberg acknowledges Scania CV for the opportunity to carry out his doctoral work at KTH Mechanics within the Linné Flow Centre.

References

[1] K. Angele, F. Grewe, Instantaneous behavior of streamwise vortices for turbulent boundary layer separation control. J. Fluids Eng. 129 (2007) 226–235.
[2] K.P. Angele, B. Muhammad-Klingmann, The effect of streamwise vortices on the turbulence structure of a separating boundary layer. Eur. J. Mech. B/Fluids 24 (2005) 539–554.
[3] K.P. Angele, B. Muhammad-Klingmann, A simple model for the effect of peak-locking on the accuracy of boundary layer statistics in digital PIV. Exp. Fluids 38 (2005) 341–347.
[4] K.P. Angele, B. Muhammad-Klingmann, PIV measurements in a weakly separating and reattaching turbulent boundary layer. Eur. J. Mech. B/Fluids 25 (2006) 204–222.
[5] P. Dengel, H.H. Fernholz, An experimental investigation of an incompressible turbulent boundary layer in the vicinity of separation. J. Fluid Mech. 212 (1990) 615–636.
[6] G. Godard, M. Stanislas, Control of a decelerating boundary layer. Part 1: Optimization of passive vortex generators. Aerosp. Sci. Technol. 10 (2006) 181–191.
[7] R. Keane, R. Adrian, Theory of cross-correlation in PIV. Appl. Sci. Res. 49 (1992) 191–215.
[8] J.C. Lin, Review of research on low-profile vortex generators to control boundary-layer separation. Prog. Aerosp. Sci. 38 (2002) 389–420.
[9] J.C. Lin, F.G. Howard, G.V. Selby, Turbulent flow separation control through passive techniques, AIAA-89–0976. in: AIAA Second Shear Flow Conference, 1989.
[10] B. Lindgren, A.V. Johansson, Evaluation of a new wind-tunnel with expanding corners. Exp. Fluids 36 (2004) 197–203.
[11] O. Lögdberg, K. Angele, P.H. Alfredsson, On the scaling of turbulent separating boundary layers. Phys. Fluids 20 (2008) 075104.
[12] J.H.M.O. Lögdberg, P.H. Fransson, Alfredsson, On the streamwise evolution of longitudinal vortices in a turbulent boundary layer. J. Fluid Mech 623 (2009) 27–58.
[13] W.R. Pauley, J.K. Eaton, Experimental study of the development of longitudinal vortex pairs embeddedd in a turbulent boundary layer. AIAA J. 26 (1988) 816–823.
[14] H.H. Pearcy, Boundary Layer and Flow Control, Its Principle and Applications Chap., In: Shock-induced Separation and Its Prevention, vol. 2. Pergamon, 1961, pp. 1170–1344
[15] M. Raffel, J. Willert, J. Kompenhans, Particle Image Velocimetry. A Practical Guide. Springer-Verlag, 1997.
[16] G. Schubauer, W. Spangenberg, Forced mixing in boundary layers. J. Fluid Mech. 8 (1960) 10–32.
[17] F. Smith, Theoretical prediction and design for vortex generators in turbulent boundary layers. J. Fluid Mech. 270 (1994) 91–131.
[18] R.V. Westphal, J.K. Eaton, W.R. Pauley, Interaction between a vortex and a turbulent boundary layer in a streamwise pressure gradient. in: F. Durst, B.E. Launder, J.L. Lumley, F.W. Schmidt, J.H. Whitelaw (Eds.), Turbulent Shear Flows 5. Springer, 1987, pp. 266–277.